

# Modeling turbulent mixing in inertial confinement fusion implosions

YAIR SREBRO,<sup>1,2</sup> DORON KUSHNIR,<sup>2,3</sup> YONI ELBAZ,<sup>1,2</sup> AND DOV SHVARTS<sup>1,2,4</sup>

<sup>1</sup>Department of Physics, Ben-Gurion University, Beer-Sheva, Israel

<sup>2</sup>Department of Physics, Nuclear Research Center–Negev, Israel

<sup>3</sup>Department of Physics, Hebrew University, Jerusalem, Israel

<sup>4</sup>Department of Mechanical Engineering, Ben-Gurion University, Beer-Sheva, Israel

(RECEIVED 29 May 2002; ACCEPTED 4 April 2003)

## Abstract

Recent direct drive implosion experiments, performed on the OMEGA laser, have been analyzed by comparing full two-dimensional (2D) and one-dimensional (1D) numerical simulations. The 2D simulations result in a fusion yield higher than experimental results. A simple full-mixing model, leaving only the clean region, overestimates yield degradation. Fully turbulent mixing is expected to develop in most of the mixing region; however regions slightly beyond the radius of the most penetrating spike are expected to remain clean and to contribute to fusion yield. One can correct the mixing model by redefining the clean region. Accounting for this unmixed region results in improved agreement with experimental results. Differences in central pressure, density, temperature, and fusion rate in implosions dominated by low mode number perturbations imply that mix effects might not be limited to the mix region, and that 2D simulations are necessary to describe the large scale flow affecting the central region. The same analysis has been undertaken for implosions with different convergence ratios, but with similar initial perturbation spectra. These implosions should be compared to implosions dominated by high mode number perturbations, which might be described by models based on 1D simulations.

**Keywords:** Direct numerical simulations; Hydrodynamic instabilities; Inertial confinement fusion; Secondary instabilities; Turbulent mixing

## 1. INTRODUCTION

A series of high uniformity spherical implosion experiments has recently been conducted on the OMEGA laser system in the University of Rochester (Marshall *et al.*, 2000; Meyerhofer *et al.*, 2001). In these experiments, 3–15 atm deuterium ( $D_2$ )-filled plastic shells of diameter  $\sim 1$  mm were irradiated with 1-ns square laser pulses of total energy  $\sim 20$  kJ. Fusion yields were measured experimentally to be 10–50% of one-dimensional (1D) numerical simulations' prediction. It is believed this is mainly due to core–shell mixing.

Unlike full-scale inertial confinement fusion (ICF) implosions, which aim to attain a self-sustaining fusion reaction (Lindl, 1995), the experiments under consideration here are scaled down to the energy of the OMEGA laser system, and are not planned to achieve ignition. The fusion rate in these experiments depends strongly on the spherical sym-

metry of converging shock waves, which heat and compress the gas. Therefore, the effect of perturbations and of turbulent mixing on these implosions is different than their effect on ICF ignition, as has been investigated by Kishony and Shvarts (2001).

During the shell acceleration, a wide spectrum of perturbations reaches the inner shell interface, and then grows due to the Rayleigh–Taylor instability (RTI) during the deceleration (Sharp, 1984; Lindl, 1995). The perturbations in these implosions include inner and outer surface roughness, beam-to-beam power imbalance, and single-beam laser nonuniformity, which has been reduced to a minimal level using 1 THz two-dimensional smoothing by spectral dispersion (2D-SSD; Skupsky *et al.*, 1989). During the acceleration stage, perturbations on the outer interface of the shell grow due to the ablative RTI and feed-through to the inner interface. The most dominant inner surface perturbation at the beginning of the deceleration originates from power imbalance, which has a spherical mode number of  $\sim 6$ –10. Shorter wavelength perturbations are stabilized by the ablation, and their feed-through is less effective.

Address correspondence and reprint requests to: Yair Srebro, Department of Physics, Nuclear Research Center–Negev, P.O. Box 9001, 84190, Israel. E-mail: yair\_srebro@hotmail.com

The RTI growth of these perturbations during the deceleration induces a strong shear in the flow, which initiates a secondary instability—the Kelvin–Helmholtz instability (KHI). The rate of nuclear fusion in the mix region is reduced due to cooling down of the hot gas when mixed with the cold plastic shell. Moreover, if fully developed turbulence is reached, mixing occurs down to the atomic scale, and the effective gas density is reduced, hence reducing the fusion rate. Direct numerical simulations describe only structures larger than the computational mesh size and normally do not include a physical mechanism causing mixing on smaller scales. Therefore, they describe the cooling of the gas only partially and do not describe the decrease in gas density. This calls for further modeling of the fully mixed region and of the fusion reactions in it. Empirical modeling of turbulent mixing is based either on two-phase flow (Youngs, 1984, 1989, 1994) or on dissipation of kinetic energy (Gauthier & Bonnet, 1990). A simple bounding estimate for the yield degradation, valid in the short wavelength limit, is obtained by assuming there are no fusion reactions in the mix region (Levedahl & Lindl, 1997).

The neutron yield degradation is customarily quantified by the ratio between the experimental yield and the yield in a one-dimensional (1D) simulation without mixing, and is denoted “yield over clean” (YOC). It has been realized that the convergence ratio (CR) of the implosion is one of the central factors determining the growth of a mix region, which in turn determines the YOC (Marshall *et al.*, 2000, Meyerhofer *et al.*, 2001, Radha *et al.*, 2002). We chose to concentrate on two typical experiments, which represent two extreme CRs. The experimental data is summarized in Table 1. The 3-atm case has a larger CR than the 15-atm case, implying more mix growth, hence a smaller YOC. This article attempts to explain both the YOC values and their dependence on the CR using these two specific experiments. Because the shell diameter and thickness and the laser conditions are similar in both experiments, the acceleration stage is similar. This implies similar perturbation growth and feed-through up to the deceleration stage, and allows a comparison mostly of the RTI unstable deceleration stage and fusion.

**Table 1.** Modeling turbulent mixing in ICF. Summary of data for the two experiments under consideration in the paper.

	Experiment 1	Experiment 2
D <sub>2</sub> pressure [atm]	15	3
Radius [ $\mu\text{m}$ ]	467	486
Shell thickness [ $\mu\text{m}$ ]	19.1	19.8
CR	14.9	34.9
Y <sub>1D</sub>	4.71e11	2.03e11
Y <sub>exp</sub>	1.60e11	4.17e10
YOC	0.34	0.21

## 2. HYDRODYNAMIC SIMULATIONS

The growth of perturbations due to the RTI is calculated using full two-dimensional (2D) hydrodynamic simulations with LEEOR2D. The simulations include separate temperatures for the ions and the electrons, a Thomas–Fermi equation of state for the electrons, and an ideal gas equation of state for the ions, electron heat conduction, and fusion reactions. The perturbation growth and feed-through during the acceleration stage is calculated using a postprocessor developed by Goncharov *et al.* (2000). The 2D simulations begin at the end of the acceleration stage by imposing on a 1D radial profile this multimode spectrum of perturbations as a modulation in the velocity field.

The result of a 1D spherical symmetric simulation with LEEOR2D for the 15-atm case is displayed in Figure 1. A first shock converges to the center at  $t \sim 1.6$  ns, and causes an initial rise in the neutron production rate to  $\sim 3e19 \text{ s}^{-1}$ . This shock reflects from the center, hits the shell interface at  $t \sim 1.7$  ns, and then converges again to the center at  $t \sim 1.8$  ns, causing a second rise in the neutron production rate to  $\sim 1e21 \text{ s}^{-1}$ . A third weaker shock converges to the center at  $t \sim 1.9$  ns, and raises the neutron production rate to the maximal level of  $\sim 4e21 \text{ s}^{-1}$ . Figure 2 displays the result of the 2D simulation for this 15-atm implosion, including the full spectrum of perturbations. Up to  $t \sim 1.7$  ns, the shell is quite symmetric, however from  $t = 1.8$  ns, the growth of perturbations can be clearly seen. These perturbations are dominated by mode number 6, which originates mostly from power imbalance. By  $t = 2$  ns, the cold plastic spikes almost reach the center of the hot gas bubble. Because the peak of the fusion rate is at  $t \sim 1.9$ – $2$  ns, these perturbations are expected to have a large effect on the neutron yield. Figure 3 displays the result of the 2D simulation for the 3-atm case, in which perturbation growth is qualitatively similar. How-

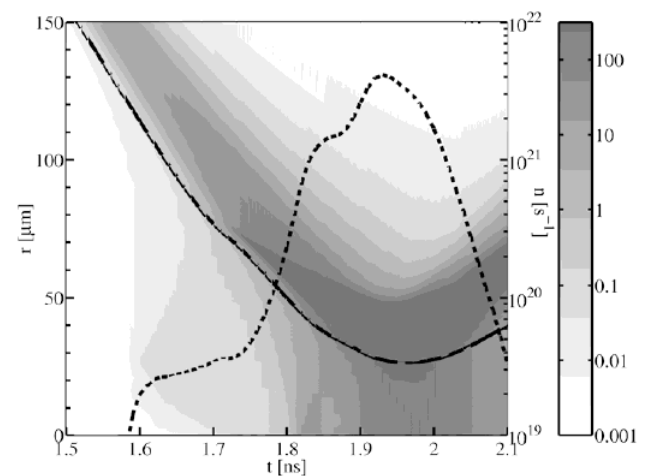


**Fig. 1.** Result of a 1D simulation for the 15-atm case. The colormap denotes density [ $\text{gr}/\text{cm}^3$ ] versus radius and time. Also plotted are the gas-shell interface (solid line) and the neutron production rate on a logarithmic scale (dashed line).

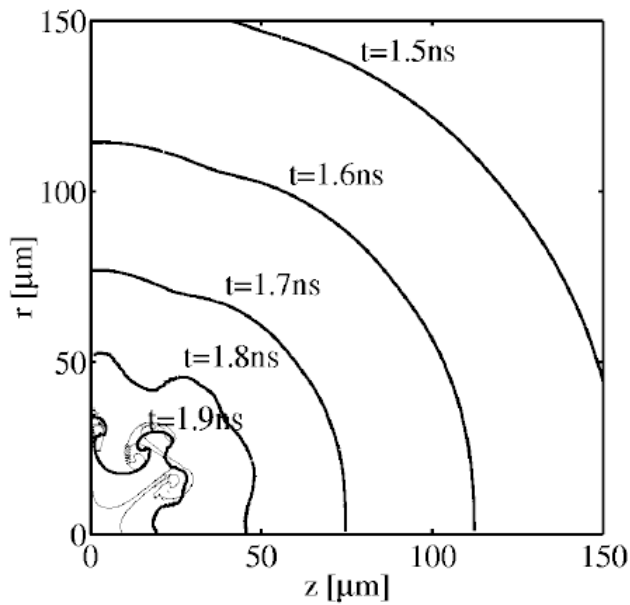


Fig. 2. Temporal evolution of gas-shell interface in a 2D simulation of the 15-atm case. The thin line corresponds to  $t = 2$  ns, when peak neutron production occurs.

ever, due to the smaller gas pressure, the stagnation is at a smaller radius and the mixing zone grows to a larger extent.

Neutron yield is smaller in 2D simulations as compared to the 1D simulations, as can be seen for both implosions in Figure 4. When the first shock emerges from the shell interface it is nearly unperturbed. Thus, the shock converges very symmetrically, and the rise it causes to the neutron

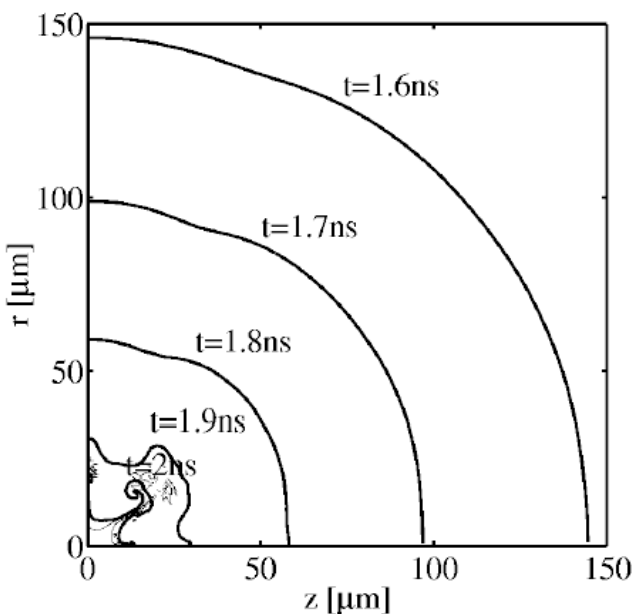


Fig. 3. Temporal evolution of gas-shell interface in a 2D simulation of the 3-atm case. The thin line corresponds to  $t = 2.1$  ns, when peak neutron production occurs.

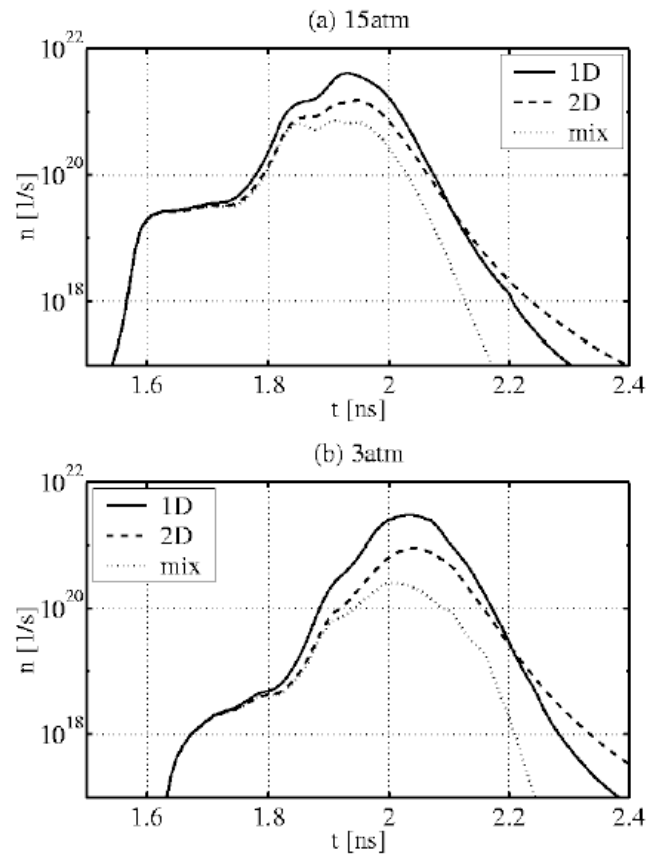


Fig. 4. Neutron production rate versus time for (a) 15 atm and (b) 3 atm. Plotted are the results of 1D simulations (solid lines), of 2D simulations (dashed lines), and of 2D simulations with the simple mixing model (dotted lines).

production rate is not affected by the perturbations. By the time the first shock is reflected from the center and reaches the interface again there is a small perturbation on the interface. Hence, the second shock reflected from the interface and converging to the center is slightly perturbed. This results in a reduction of the second rise in the neutron production rate by a factor of  $\sim 2$ . When the second shock reaches the interface, it has a large perturbation on it, and the convergence of the third shock is strongly affected. The sharp rise in the neutron production rate at the convergence of the third shock to the center can hardly be seen in the 2D simulations. The maximal neutron production rate is reduced by a factor of 2.7 for the 15-atm case and by a factor of 3.4 for the 3-atm case. The integrated neutron yield is reduced by a factor of  $\sim 2$  for the 15-atm case and by a factor of  $\sim 3$  for the 3-atm case.

These simulations describe the mixing between the gas and the shell only on length scales larger than the computational mesh size. To describe mixing of smaller structures, we define the mix region as the region between the radius,  $R_{spike}$ , of the spike that has penetrated most deeply into the gas, and the radius,  $R_{bubble}$ , of the bubble that has penetrated most deeply into the shell. Following the 1D modeling of

Levedahl and Lindl (1997), we assume this entire region is fully mixed due to secondary instabilities. The full-mixing model is attained from the 2D simulations by assuming fusion reactions only in the central clean region. This model results in a reduction in the total neutron yield by another factor of  $\sim 2$  for the 15-atm case and by a factor of  $\sim 3$  for the 3-atm case. The reduction due to this model grows with time due to the growth of the extent of the mix region, as can be seen in Figure 4.

These results are summarized and compared to the experimental results for the two implosions in Figure 5. The 2D simulations underestimate yield degradation, and the simple mixing model overestimates it. However the CR dependence of both the 2D simulations without mixing and with the simple mixing model is similar to that found in the experiments. For the 15-atm case, which has a smaller CR, the yield resulting from the simple mixing model is lower by a factor of  $\sim 2$  than the yield assuming no mixing. This reflects the fact that half of the yield is from the mix region and half from the clean region. For the 3-atm case the yield is reduced by a factor of  $\sim 3$ , indicating that only one-third of the yield in the 2D simulation is from the clean region.

### 3. ANALYSIS OF SIMULATIONS

To analyze the differences between the 1D and 2D simulations, we define the cumulative fusion rate as the spatial integral of the fusion rate:

$$N(R, t) = \int_0^R n(\mathbf{r}, t) d^3 \mathbf{r}, \quad (1)$$

where  $n(\mathbf{r}, t)$  is the fusion rate as a function of the location vector,  $\mathbf{r}$ , and time,  $t$ . Figure 6 displays  $N(R)$  for the 1D and the 2D simulations for the two cases at the peak neutron production rate. Simulation results are normalized to the 1D neu-

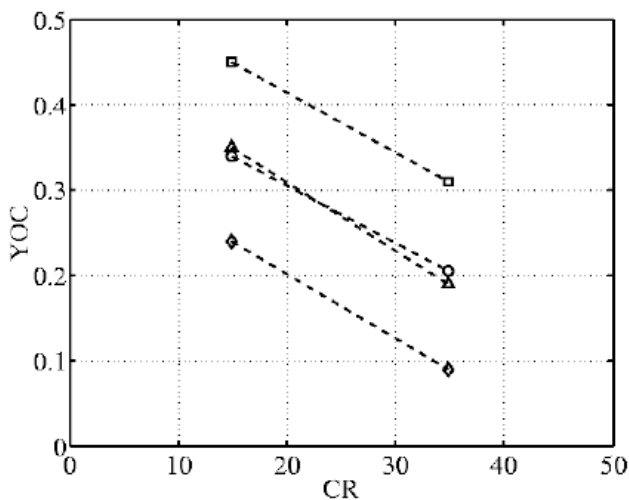


Fig. 5. YOC versus CR for experiments (circles), 2D simulations (squares), simple mixing model (diamonds), and modified mixing model (triangles).

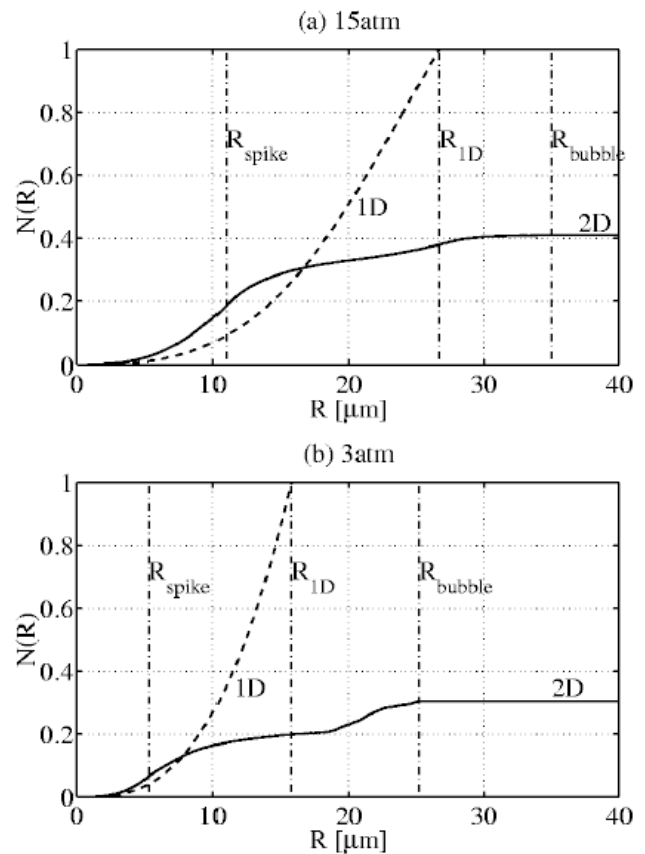


Fig. 6. The cumulative fusion rate normalized to the 1D rate versus radius for (a) the 15-atm case at  $t = 1.95$  ns and (b) the 3-atm case at  $t = 2.05$  ns. The 2D simulations (solid line) are compared to the 1D simulations (dashed line). The vertical lines denote  $R_{1D}$ ,  $R_{bubble}$ , and  $R_{spike}$ .

tron rate. In the 1D simulation,  $N(R)$  is a smooth rising function. In 2D, we observe several features. The central region is clean and behaves qualitatively like the whole 1D bubble; however, the yield from it is higher than the yield from the same region in the 1D simulation. This feature can more clearly be seen for the 15-atm case. The rise in the cumulative fusion rate in the central region ends gradually at a radius slightly larger than  $R_{spike}$ . Then, throughout most of the mix region there is a small contribution to the cumulative fusion rate, and before  $R_{bubble}$  there is a second rise due to the gas bubbles that have penetrated the plastic shell due to the RTI.

Perturbations change the dynamics of shock waves during the compression, and generally cause them to be less sharp and to converge less singularly to the center, hence degrading efficiency of heating and compression. On the other hand, due to these nonsharp shocks, the entropy remains lower than in 1D, allowing for a more efficient compression. The higher yield from the central region in 2D results from a higher density attained there. These differences in central pressure, density, and fusion rate imply that mix effects are not limited to the mix region, and may not be described by effective 1D mix models. This occurs for the specific implosions under consideration here, which had

high perturbation amplitudes and were dominated by low mode numbers.

The smaller slope of  $N(R)$  in the mixing region is partly because less gas mass is present there and partly because fewer fusion reactions occur in this mass. To separate these two effects, we plot in Figure 7 the cumulative fusion rate at the peak neutron production rate as a function of cumulative mass:

$$m(R, t) = \int_0^R \rho_{gas}(\mathbf{r}, t) d^3 \mathbf{r}, \quad (2)$$

where  $\rho_{gas}(\mathbf{r}, t)$  is the gas density as a function of  $\mathbf{r}$  and  $t$ .

The central 20–25% of the mass behaves similarly in 1D and in 2D, implying that the difference in the central region observed above was mainly due to flow of more mass into the center and not from a change in the fusion rate per unit mass. For the rest of the gas there is a gradual increase in the cumulative fusion rate at a smaller rate compared to 1D. This reduced fusion rate per unit mass is purely due to the presence of the perturbations, and not due to less mass being present as may be inferred from the radial profiles presented

in Figure 6. These features of mass flow into the center and of thin tubes connecting the bubbles to the central clean region may be typical only for implosions dominated by long-wavelength perturbations. Whenever such differences between the 1D and 2D radial profiles occur, care should be taken when combining models for calculating the extent of the mix region with 1D simulations. The behavior of the fusion rate as a function of mass implies that in such modeling it is more important to reproduce the correct mass distribution than the correct radial distribution.

#### 4. ESTIMATES OF MIXING

We expect the secondary instabilities to cause turbulent mixing in the region occupied by the large-scale bubbles and spikes generated by the RTI. Figure 8 displays the gas shape at peak compression with the vorticity of the flow, defined as  $\boldsymbol{\omega} = \nabla \times \mathbf{u}$ , where  $\mathbf{u}$  is the velocity vector. The KHI is expected to grow as,  $d_{KH} \approx 0.1 \Delta u \Delta t$  (Brown & Roshko, 1974), where  $\Delta u = \omega \Delta x$  is the shear in the velocity,  $\Delta x$  is the typical length scale of the shear, and  $\Delta t$  is the time scale for the instability growth. In this case,  $\omega$  reaches  $100 \text{ ns}^{-1}$  and  $\Delta t \approx 0.1 \text{ ns}$ ; therefore  $d_{KH} \approx \Delta x$ . This means that we should expect the vortices to grow to the size of the perturbation scale described in the simulations, and regions with high vorticity are expected to be mixed due to the KHI. The simple full-mixing model defines  $R_{clean} = R_{spike}$  and assumes all the regions with  $r > R_{clean}$  are fully mixed. This definition does include all the region between the bubbles and the spikes, but also includes the wide bases of the bub-

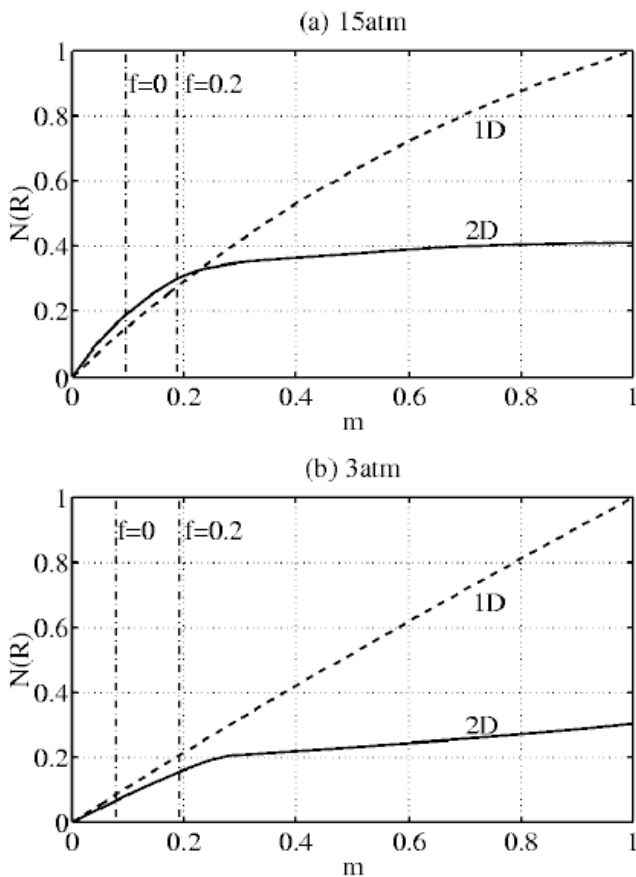


Fig. 7. The cumulative fusion rate normalized to the 1D rate versus mass for (a) the 15-atm case at  $t = 1.95 \text{ ns}$  and (b) the 3-atm case at  $t = 2.05 \text{ ns}$ . The 2D simulations (solid line) are compared to the 1D simulations (dashed line). The vertical lines denote  $R_{clean}$  for  $f = 0$  ( $R_{clean} = R_{spike}$ ) and  $f = 0.2$ .

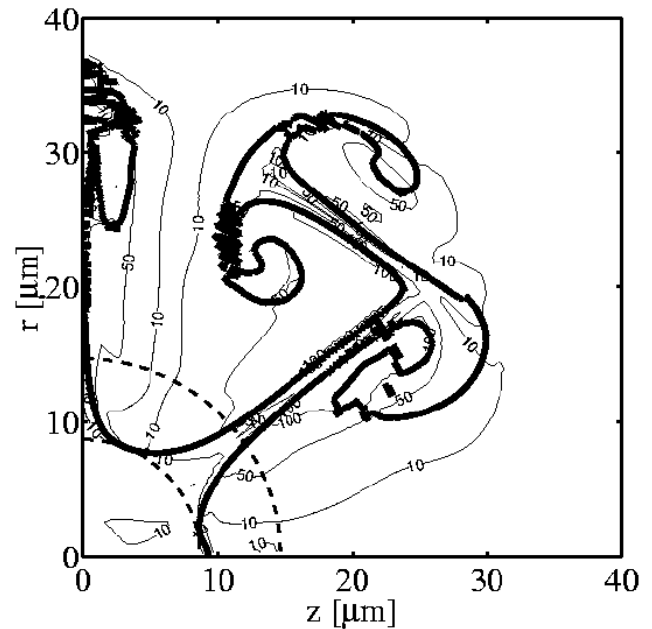


Fig. 8. Contours of vorticity [ $\text{ns}^{-1}$ ] for the 15-atm case at  $t = 2 \text{ ns}$ . The thick solid line denotes the gas-shell interface and the two dashed circles denote the simple ( $f = 0$ ) and modified ( $f = 0.2$ ) definitions for the clean region.

bles, where the shear in the velocity is smaller by an order of magnitude than the shear in the expected mix region. Regions with such small shear are not expected to be mixed due to the KHI. Without a detailed mixing model based on KHI, we suggest a simple crude estimate by defining the mix region with  $R_{clean}$  slightly larger than  $R_{spike}$ . In this manner only the expected mix region will be included, and the expected clean region will not be affected by the mixing model. Figure 8 demonstrates how increasing  $R_{clean}$  slightly results in a good definition of the mixing region.

We now define  $R_{clean} = R_{spike} + f(R_{bubble} - R_{spike})$ , where  $f$  is a free parameter. Figure 9 displays the YOC as a function of this parameter,  $f$ . There is a dramatic rise in the YOC value around  $f = 0$ , which corresponds to the simple mixing model. This rise continues up to  $f \sim 0.2$ , where the tubes connecting the bubbles to the central region get very thin. The second rise from  $f \sim 0.7$  to  $f = 1$  (no small-scale mixing) is due to the bubbles. If we assume the bubbles and the tubes connecting them to the central region are fully mixed, we should define  $R_{clean}$  with  $f \sim 0.2$ . A correction to the mixing model is suggested by choosing the value of  $f$ , where the bubbles' bases end and where the steep rise in the YOC ends. In both implosions under consideration here, a value of  $f \sim 0.2$  should be taken. This single value of  $f$  identifies the high vorticity zones for both implosions because both have similar spectra of perturbations and similar vorticity maps. This is not a general result, and it should be reconsidered for every specific implosion and perturbation spectrum.

We modify the mixing model by taking  $f = 0.2$ . In this manner only the regions theoretically expected to be mixed are included, and the YOC values are between the overestimate of the 2D simulation without mixing to the simple

mixing model. The modified YOC values are in good agreement with the experimental results, as can be seen in Figure 5.

## 5. CONCLUSIONS

Recent ICF experiments have been analyzed by comparing the experimental results with full 1D and 2D numerical simulations for implosions with two extreme CRs. Differences in central pressure, density, and fusion rate at high perturbation amplitudes imply that mix effects are not limited to the mix region, so that care should be taken when describing them by effective 1D mix models. Assuming no mixing beyond the length scales described in the 2D simulations, the bubbles raise fusion yield above experimental results, whereas assuming a simple full-mixing model overestimates yield degradation. The problem with the simple mixing model is that regions slightly beyond the clean radius contribute significantly to fusion yield, while they are expected not to be mixed due to the KHI. The mixing model is therefore modified by redefining the clean radius according to crude estimates based on vorticity maps in the 2D simulations, resulting in improved agreement with experimental results for a wide range of CRs.

The implosions investigated in this paper were dominated by low mode number perturbations, originating mainly from power imbalance between the various laser beams. This implies a difficulty in describing both the mix region and the central clean region by effective 1D models. Implosions with a reduction in this perturbation have been investigated by 2D simulations, and were found to behave differently. The perturbations generated by the RTI have a wider spectrum of mode numbers, so that bubble competition plays a central role in driving the evolution into a self-similar regime, where effective models for the calculation of the mix region may again be applied. Moreover, for implosions dominated by high mode number perturbations less large-scale flow into the central region is expected, and 1D simulations together with models such as that of Levedahl and Lindl (1997) may be adequate to describe the turbulent mixing.

It has been found that perturbations cause shock waves to be less sharp; hence, the entropy remains lower and the compression of the central region is more effective. This effect causes it to differ from the corresponding symmetric implosion. This effect should be further investigated both for these implosions and for more general cases.

Simulations and modeling of mixing were compared to experiments through one measured parameter—the neutron yield. However, more parameters, such as fuel areal density and temperature may be deduced from the experiments and compared to theoretical models, as has been done by Meyerhofer et al. (2001) and by Radha et al. (2002).

All mix analysis has been conducted as a postprocessing of the hydrodynamic simulations. In reality, the evolution of the turbulent mixing affects the large-scale dynamics and should be taken into account with a feedback to the hydro-

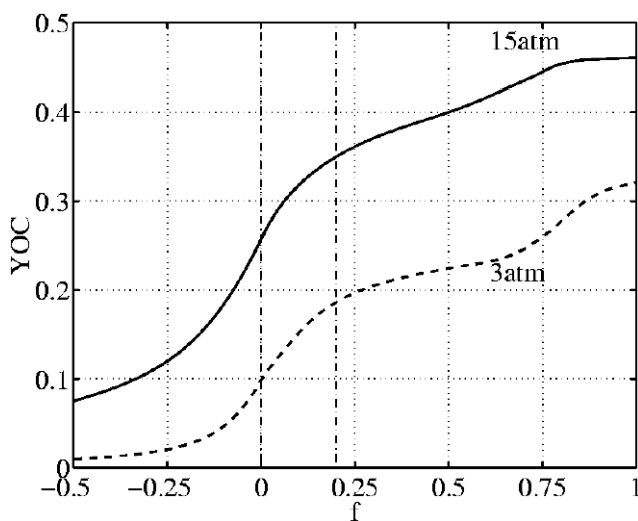


**Fig. 9.** YOC versus  $f$ , where  $f$  defines  $R_{clean}$  as  $R_{clean} = R_{spike} + f(R_{bubble} - R_{spike})$ . The solid line represents the 15-atm case and dashed line represents the 3-atm case. The vertical lines denote the simple ( $f = 0$ ) and modified ( $f = 0.2$ ) definitions for the clean region.

dynamic simulation. In this manner the level of mixing in every region may be evaluated more precisely.

## ACKNOWLEDGMENTS

The authors thank the Laboratory for Laser Energetics at the University of Rochester for their hospitality and partial support during this work. Special thanks are given to D.D. Meyerhofer and P.B. Radha for supplying the experimental results, to V.N. Goncharov and P. McKenty for generating initial conditions for the simulations, and to D. Oron for helpful remarks.

## REFERENCES

- BROWN, G.L. & ROSKOPF, A.J. (1974). On the density effects and large structure in turbulent mixing layers. *J. Fluid Mech.* **64**, 775–816.
- GAUTHIER, S. & BONNET, M. (1990). A k-epsilon model for turbulent mixing in shock-tube flows induced by Rayleigh–Taylor instability. *Phys. Fluids A*, **2**, 1685–1694.
- GONCHAROV, V.N., MCKENTY, P., SKUPSKY, S., BETTI, R., MCCRORY, R.L. & CHERFILS-CLEROUIN, C. (2000). Modeling hydrodynamic instabilities in inertial confinement fusion targets. *Phys. Plasmas* **7**, 5118–5139.
- KISHONY, R. & SHVARTS, D. (2001). Ignition condition and gain prediction for perturbed inertial confinement fusion targets. *Phys. Plasmas* **8**, 4925–4936.
- LEVEDAHL, W.K. & LINDL, J.D. (1997). Energy scaling of inertial confinement fusion targets for ignition and high gain. *Nucl. Fusion* **37**, 165–173.
- LINDL, J.D. (1995). Development of the indirect-drive approach to inertial confinement fusion and the target physics basis for ignition and gain. *Phys. Plasmas* **2**, 3933–4024.
- MARSHALL, F.J., DELETTREZ, J.A., EPSTEIN, R., GLEBOV, V.YU., HARDING, D.R., MCKENTY, P.W., MEYERHOFER, D.D., RADHA, P.B., SEKA, W., SKUPSKY, S., SMALYUK, V.A., SOURES, J.M., STOECKL, C., TOWN, R.P.J., YAAKOBI, B., LI, C.K., SEGUIN, F.H., HICKS, D.G. & PETRASSO, R.D. (2000). Direct-drive high-convergence-ratio implosion studies on the OMEGA laser system. *Phys. Plasmas* **7**, 2108–2113.
- MEYERHOFER, D.D., DELETTREZ, J.A., EPSTEIN, R., GLEBOV, V.YU., GONCHAROV, V.N., KECK, R.L., MCCRORY, R.L., MCKENTY, P.W., MARSHALL, F.J., RADHA, P.B., REAGAN, S.P., ROBERTS, S., SEKA, W., SKUPSKY, S., SMALYUK, V.A., SORCE, C., STOECKL, C., SOURES, J.M., TOWN, R.P.J., YAAKOBI, B., ZUEGEL, J.D., FRENJE, J., LI, C.K., PETRASSO, R.D., SEGUIN, F.H., FLETCHER, K., PADALINO, S., FREEMAN, C., IZUMI, N., LERCHE, R., PHILLIPS, T.W. & SANGSTER, T.C. (2001). Core performance and mix in direct-drive spherical implosions with high uniformity. *Phys. Plasmas* **8**, 2251–2256.
- RADHA, P.B., DELETTREZ, J., EPSTEIN, R., GLEBOV, V.YU., KECK, R., MCCRORY, R.L., MCKENTY, P., MEYERHOFER, D.D., MARSHALL, F., REAGAN, S.P., ROBERTS, S., SANGSTER, T.C., SEKA, W., SKUPSKY, S., SMALYUK, V., SORCE, C., STOECKL, C., SOURES, J., TOWN, R.P.J., YAAKOBI, B., FRENJE, J., LI, C.K., PETRASSO, R., SEGUIN, F., FLETCHER, K., PADALINO, S., FREEMAN, C., IZUMI, N., LERCHE, R. & PHILLIPS, T.W. (2002). Inference of mix in direct-drive implosions on OMEGA. *Phys. Plasmas* **9**, 2208–2213.
- SHARP, D.H. (1984). An overview of Rayleigh–Taylor instability. *Physica D* **12**, 3.
- SKUPSKY, S., SHORT, R.W., KESSLER, T., CRAXTON, R.S., LETZRING, S. & SOURES, J.M. (1989). Improved laser-beam uniformity using the angular dispersion of frequency-modulated light. *J. Appl. Phys.* **66**, 3456–3462.
- YOUNGS, D.L. (1984). Numerical simulation of turbulent mixing by Rayleigh–Taylor instability. *Physica D* **12**, 32–44.
- YOUNGS, D.L. (1989). Modelling turbulent mixing by Rayleigh–Taylor instability. *Physica D* **37**, 270–287.
- YOUNGS, D.L. (1994). Numerical simulation of mixing by Rayleigh–Taylor and Richtmyer–Meshkov instabilities. *Laser Part. Beams* **12**, 725–750.